Laser-based Detection and Depth Estimation of Dry and Water-Filled Potholes: A Geometric Approach

Kiran Kumar Vupparaboina, Roopak R. Tamboli, P. M. Shenu, Soumya Jana
Department of Electrical Engineering, Indian Institute of Technology Hyderabad,
Yeddumailaram, Medak–502205, Telangana, India.
Email: {ee11p012, ee13p0008, ee10m11, jana}@iith.ac.in

Abstract—In secondary Indian roads, one often encounters potholes which can be either dry or water-filled. Accordingly, to ensure safe driving, it is imperative to detect potholes and estimate their depths in either condition. In this paper, we develop a physics-based geometric framework, where such detection and depth-estimation can be accomplished using suitable laser. Specifically, we relate dry pothole depth to measured optical deviation using simple ray optics. Further, we use Snell's law of refraction to obtain a quartic equation, and its appropriate real root to relate water-filled pothole depth to the corresponding optical deviation. Here we take into account diminishing resolution with increasing distance from the camera. We conclude by experimentally validating our method.

Index Terms—Vehicular safety, dry and water-filled potholes, pothole detection, pothole depth estimation

I. INTRODUCTION

Recent advances in vehicular safety and driver assistance technology have greatly reduced the burden of driving. Examples include collision warning, localization, cooperative driving, and driverless vehicles, which has been enabled by vehicular communication [1]. Yet, vast developing markets, such as India, are yet to benefit adequately from such advances, because certain specific concerns remain unaddressed. For example, in countries such as India, one often encounters secondary roads dotted with potholes, which can get filled with water during monsoon (Fig. 1). Detecting potholes and estimating their depth, especially, when water-filled, with bare eyes while driving at night or in low light condition places undue burden on the driver. In this paper, we provide the theoretical underpinnings for filling this gap by proposing a laser-based system. Specifically, we present a physics-based geometric analysis of the problem, and validate it experimentally (in a scaled down setup).

Several attempts have been made at addressing related concerns. For instance, Pothole Patrol system proposed by Eriksson *et al.* uses accelerometer data and GPS sensors to identify potholes and other irregularities on the road surface [2]. A similar kind of pothole detection system that uses Android smartphones with accelerometers is proposed by Menis *et al.* [3]. Rode *et al.* use accelerometers and Wi-Fi enabled vehicles for pothole detection and warning system [4]. Shonil developed an FPGA based image processing system for pothole detection [5]. Yu *et al.* utilized a red laser and a camera under laser frequency to capture the images of cracks

Fig. 1: Potholes on Indian road: dry (left) and water-filled (right)

and potholes on the pavement [6]. However, these frameworks have been developed generally with high-quality roads in view and are limited only up to detection of potholes. Hence it is imperative that such potholes are not only detected, but their depths are also estimated in both dry and water-filled condition.

In this backdrop, we propose a physics-based geometric approach for detection and depth estimation of dry and water-filled potholes. We assume a camera and a laser source, ideally, with a wavelength that suffers low attenuation in water. The laser source projects a line onto the road surface. Deformation of the laser line seen by the camera is utilized for detection and depth estimation. While this problem is straightforward for dry potholes, estimating the depth of water-filled potholes is considerably more involved, for which we provide a rigorous mathematical analysis. Further, we validate our theory in a scaled-down laboratory setup, where depth of dry potholes is estimated with an accuracy greater than 98%. In contrast, depth estimation accuracy for water-filled potholes is only upto 94.7%. The curvature of water due to surface tension, especially prominent in our scaled down setup, appears to contribute to the reduction in accuracy in the water-filled scenario.

The rest of this paper is organized as follows. Section II discusses the proposed geometric approach for finding physical depth of both dry and water filled potholes. Creation of reference data for the prototype used is explained in section III. Section IV gives the experimental details and observations, and finally we conclude in section V.

II. DETECTION AND DEPTH ESTIMATION

We consider a camera-laser arrangement mounted on the vehicle to sense the presence of pothole. Fig.2 shows the
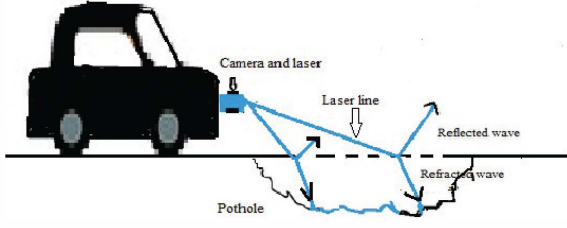
Fig. 2: Schematic of pothole sensing system.

schematic of the proposed setup. Camera is placed on top of the laser such that it captures the light projected by the laser. We chose laser source to be a line laser so that when illuminated, camera sees a straight line on the normal road surface. However, in the presence of pothole, laser line undergoes deformation which is captured by the camera. Detection and measurement of this deviation is automated using basic image processing based on template matching. Maximum deviation measured indicates the deepest point in the pothole, which is further used to estimate the depth of pothole. Note that laser deviation will be less in water-filled pothole as compared to dry pothole, due to refraction of light, making depth calculation challenging. In this setting, we present physics based geometrical analysis for estimation of depth of both dry and water-filled potholes.
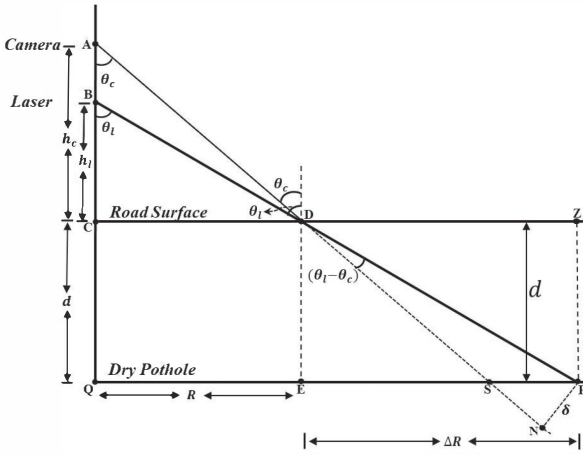
A. Dry Pothole

Fig. 3: Geometrical depiction of dry pothole.

d	:	Real depth
δ	:	Displacement dry pothole
θ_c	:	Angle of inclination of camera
θ_l	:	Angle of inclination of laser
R	:	Range of laser ray on normal road surface
ΔR	:	Increment in range due to presence of pothole
l	:	Length of line segment DP

We first present the analysis for dry pothole. Ray diagram representation for detecting dry pothole using proposed setup

is shown in Fig. 3. Camera is placed at point A and laser at point B which is below the camera. Camera and laser are arranged to align vertically. In the absence of pothole, laser ray hits road surface at point D. Its reflection seen by the camera follows the path AD. Note that to make the analysis simpler camera is arranged such that image of point D is the principal point. In the presence of dry pothole, laser line still follows the path BD and meets the surface at P. Now, camera captures the ray from point P and parallel to principle axis. In other words, the image captured by the camera is nothing but the image of δ shown in the Fig. 3. The relation between δ and physical depth d is obtained as follows

From $\triangle$DEF, $\triangle$FDG, we get

$$\sin(\theta_l - \theta_c) = \frac{\delta}{l} \tag{1}$$

$$\cos\theta_l = \frac{d}{l}. \tag{2}$$

Dividing (2) by (1), we get

$$d = \delta\frac{\cos\theta_l}{\sin(\theta_l - \theta_c)}. \tag{3}$$

For a calibrated arrangement θ_c, θ_l, h_c, h_l and R will remain fixed. Only δ varies with respect to pothole depth. Hence, we shall assume the above mentioned parameters to be known in the further discussions.

B. Water-filled Pothole

For the water-filled potholes, the depth of the pothole obtained will be less than the real depth due to the difference in refractive index of air and water. Water being more dense than air, the laser rays entering the water will bend towards the normal. Ray diagram representation of water-filled pot-hole is shown in Fig. 4. The camera captures the image of reflected rays which give apparent depth of the pothole. The mathematical analysis is as follows.
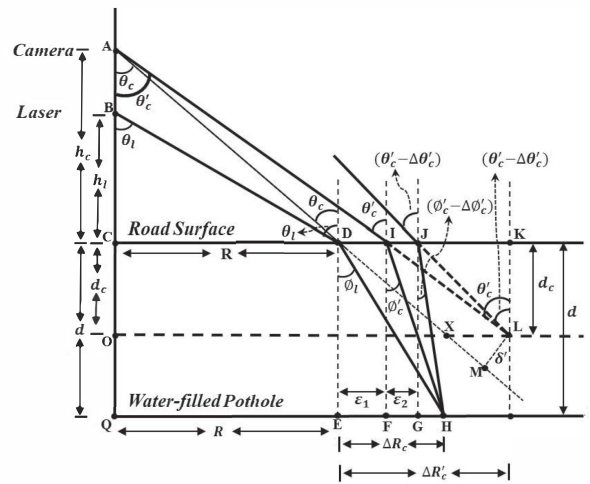

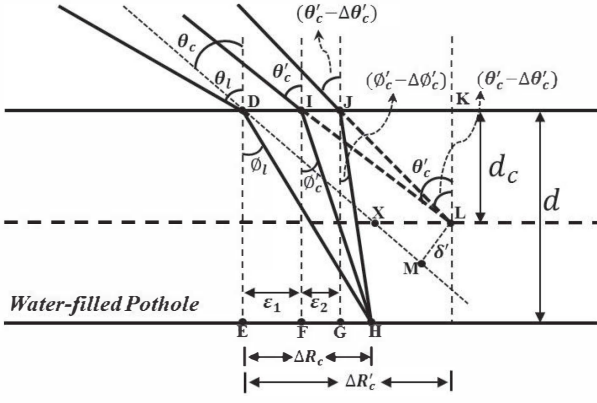Fig. 4: Geometrical depiction of water-filled pothole.

Fig. 5: Zoomed view of Fig. 4

d_c : Apparent depth considering the camera rays
δ' : Displacement seen by camera
θ_c' : Angle of incidence of reflected ray seen by camera
ϕ_c' : Angle of refraction of reflected laser ray
R : Range of laser ray on normal road surface
ΔR_c: Increment in range w. r. t d for water-filled case
$\Delta R_c'$: Increment in range w.r. t d_c

1) Basic Equations: As shown in Fig. 4 line DH is the refracted laser ray into the pothole making an angle ϕ_l with the normal. The ray hitting the bottom of the pothole is reflected back to the camera line segment HI. However, the camera images a different point (point L) due to the difference of refractive index of two media. The camera sees the point L which is at the apparent depth d_c of the pothole. In other words, the deviation captured by the camera is δ' as shown in Fig. 4. We can now obtain a relation between δ', d_c, and d as follows.

From $\triangle$DEH, $\triangle$IFH and $\triangle$JGH, we have

$$\tan(\phi_c') = \frac{\Delta R_c - \epsilon_1}{d} \tag{4}$$

$$\tan(\phi_c' - \Delta\phi_c') = \frac{\Delta R_c - \epsilon_1 - \epsilon_2}{d}. \tag{5}$$

Subtracting (4) from (5), noting $\Delta\phi_c'$ as small, and using $\frac{d(\tan x)}{dx} = \sec^2 x$, we get

$$\frac{\epsilon_2}{d} = \Delta\phi_c' \sec^2(\phi_c'). \tag{6}$$

Similarly, from $\triangle$ILK and $\triangle$JLK, we have

$$\tan\theta_c' = \frac{\Delta R_c' - \epsilon_1}{d_c} \tag{7}$$

$$\tan(\theta_c' - \Delta\theta_c') = \frac{\Delta R_c' - \epsilon_1 - \epsilon_2}{d_c}. \tag{8}$$

Again, subtracting (8) from (7), and noting $\Delta\theta_c'$ as small, we get

$$\frac{\epsilon_2}{d_c} = \Delta\theta_c' \sec^2(\theta_c'). \tag{9}$$

Dividing (6) by (9), we get

$$\frac{d_c}{d} = \frac{\Delta\phi_c'}{\Delta\theta_c'} \frac{\sec^2 \phi_c'}{\sec^2 \theta_c'}. \tag{10}$$

From Snell's law we have

$$\frac{\sin\theta_c'}{\sin\phi_c'} = \eta \tag{11}$$

$$\frac{\sin(\theta_c' - \Delta\theta_c')}{\sin(\phi_c' - \Delta\phi_c')} = \eta, \tag{12}$$

where $\Delta\theta_c'$ and $\Delta\phi_c$ are small. Therefore, noting $\sin\Delta\theta_{c'} \approx \Delta\theta_{c'}$ and $\cos\Delta\theta_{c'} \approx 1$ in (13), we obtain

$$\eta = \frac{\Delta\theta_c'}{\Delta\phi_c'} \frac{\cos\theta_c'}{\cos\phi_c'} \tag{13}$$

$$\frac{\Delta\theta_c'}{\Delta\phi_c'} = \eta \frac{\cos\phi_c'}{\cos\theta_c'}. \tag{14}$$

Substituting (14) in (10), we get

$$\frac{d_c}{d} = \frac{1}{\eta} \frac{\cos^3\theta_c'}{\cos^3\phi_c'}. \tag{15}$$

Now, to relate δ' and d_c, consider $\triangle$XLM and we have

$$\delta' = \overline{XL}\cos\theta_c. \tag{16}$$

From $\triangle$AOL and $\triangle$AOX in Fig. 4, we have

$$\overline{XL} = \overline{OL} - \overline{OX} \tag{17}$$
$$= (h_c + d_c)(\tan\theta_c' - \tan\theta_c). \tag{18}$$

Substituting (18) in (16), we get

$$\delta' = (h_c + d_c)(\tan\theta_c' - \tan\theta_c)\cos\theta_c. \tag{19}$$

Rearranging (19), we get

$$d_c = \frac{\delta'}{\cos\theta_c(\tan\theta_c' - \tan\theta_c)} - h_c. \tag{20}$$

Substituting (20) in (15) and rearranging, we get

$$d = \frac{1}{\eta^2} \left(\frac{\delta'}{\cos\theta_c(\tan\theta_c' - \tan\theta_c)} - h_c \right) \frac{\cos^3\phi_c'}{\cos^3\theta_c'}. \tag{21}$$

2) Relating θ_c' to θ_c and other parameters: For water-filled potholes, (21) relates real depth and deviation δ' by considering the multiple reflected rays seen by the camera. ϕ_c' and θ_c' in (21) are auxiliary variables which need to be eliminated by relating them to known quantities (θ_c, θ_l and h_c) and d. This can be done considering single reflected ray captured by camera (see Fig. 6).

From $\triangle$DEH and $\triangle$IFH, we have

$$\epsilon_1 = d(\tan\phi_l - \tan\phi_c'). \tag{22}$$

From $\triangle$ACD and $\triangle$ACI, we have

$$\epsilon_1 = h_c(\tan\theta_c' - \tan\theta_c). \tag{23}$$

Equating (22) and (23), we get

$$h_c(\tan\theta_c' - \tan\theta_c) = d(\tan\phi_l - \tan\phi_c'). \tag{24}$$

Rearranging (24), we get

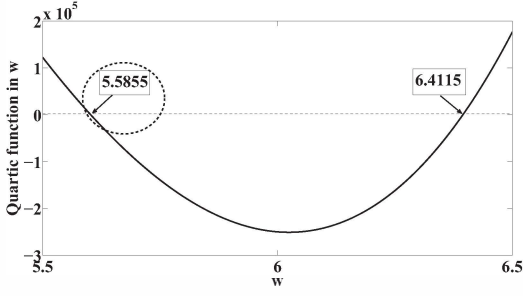$$h_c\tan\theta_c' + d\tan\phi_c' = h_c\tan\theta_c + d\tan\phi_l. \tag{25}$$

Fig. 6: Water-filled pothole considering only single reflected ray towards camera

Right hand side of (25) is in terms of auxiliary variables θ_c' and ϕ_c'. To eliminate them, we first express $\tan \phi_c'$ in terms of $\tan \theta_c'$ using Snells law as follows.

$$\sin \phi_c' = \frac{\sin \theta_c'}{\eta} \qquad (26)$$

$$\cos \phi_c' = \sqrt{1 - \sin^2 \phi_c'}. \qquad (27)$$

Substituting (26) in (27), we get

$$\cos \phi_c' = \frac{\sqrt{\eta^2 - \sin^2 \theta_c'}}{\eta} \qquad (28)$$

and similarly, we can also get

$$\tan \phi_c' = \frac{\tan \theta_c'}{\sqrt{\eta^2 + (\eta^2 - 1)\tan^2 \theta_c'}}. \qquad (29)$$

Substituting (29) in (25) and let $h_c \tan \theta_c + d \tan \phi_l = a$ in (25), we get

$$\tan \theta_c' \left[h_c + \frac{d}{\sqrt{\eta^2 + (\eta^2 - 1)\tan^2 \theta_c'}} \right] = a. \qquad (30)$$

Now let

$$w = \eta^2 + (\eta^2 - 1)\tan^2 \theta_c' \qquad (31)$$

$$\Rightarrow \tan \theta_c' = \sqrt{\frac{w - \eta^2}{\eta^2 - 1}}. \qquad (32)$$

Substituting (31) and (32) in (30), we get

$$\sqrt{\frac{w - \eta^2}{\eta^2 - 1}} \left(h_c + \frac{d}{\sqrt{w}} \right) = a. \qquad (33)$$

Removing rearranging (33) an quartic equation in w containing d as well. It can be expressed in the form

$$a_1 w^4 + b_1 w^3 + c_1 w^2 + d_1 w + e_1 = 0, \qquad (34)$$

where

$$
\begin{aligned}
a_1 &= h_c^4 \\
b_1 &= 2h_c^2 d^2 - 2h_c^4 \eta^2 - 2a^2 h_c^2 (\eta^2 - 1) - 4h_c^2 d^2 \\
c_1 &= a^4 (\eta^2 - 1)^2 + 2h_c^4 \eta^4 + d^4 - 2a^2 (\eta^2 - 1)d^2 \\
    &\quad + 2a^2 h_c^2 (\eta^2 - 1)\eta^2 + 6h_c^2 d^2 \eta^2 \\
d_1 &= 2a^2 (\eta^2 - 1)d^2 \eta^2 - 2d^4 \eta^2 - 2h_c^2 d^2 \eta^4 \\
e_1 &= d^4 \eta^4.
\end{aligned}
$$

Roots of (34) admit closed-form expressions [10]. These roots can be real or complex depending on nature of determinant. However, in this case only real positive root greater than η^2 is admissible, otherwise $\tan \theta_c'$ cannot be real (refer to (32)). The choice of w in case of multiple admissible roots is explained later.

3) Final equation for depth of water-filled pothole: Substituting (26), (27), and (28) in (21), we get

$$d = \frac{1}{\eta^2} \left[\frac{\delta'}{\cos \theta_c (\tan \theta_c' - \tan \theta_c)} - h_c \right] \times$$
$$\left[\eta^2 + (\eta^2 - 1)\tan^2 \theta_c' \right]^{\frac{3}{2}}. \qquad (35)$$

Now substituting (31) and (32) in (35), we get

$$d = \frac{1}{\eta^2} \left[\frac{\delta'}{\cos \theta_c \left(\sqrt{\frac{w - \eta^2}{\eta^2 - 1}} - \tan \theta_c \right)} - h_c \right] w^{\frac{3}{2}}. \qquad (36)$$

The right hand side of (36) contains w. Notice that closed-form expression of w will be in terms of d. Consequently, d appears on both sides of (36) which makes it difficult to obtain a closed form expression for d. In view of this, we opted representing (36) graphically for different values of d which is described later.

III. REFERENCE CHARTS

In this section, we present various reference charts required for finding depth of both dry and water-filled potholes. First, we discuss the choice of roots for quartic equation (34). Fig. 7 shows the zero crossing region of quartic function (34) for pothole of depth $d = 20$ mm, for $R = 31.5$ cm, $h_l = 5.5$ cm and $h_c = 14.5$ cm (R, h_c and h_l values chosen as per the experimental setup). It has two real roots where only one root (highlighted by dotted circle in Fig. 7) satisfies the empirical relation between d and δ'. The closed form expression for this particular root is given by r_3 in [10].

Next, as mentioned earlier we do not have closed form expression for finding d of water-filled pothole. Hence, we plotted δ' obtained for various values of d, and similarly δ for the same range d. Fig. 8 shows the plot for δ' vs d and δ vs d considering same $R = 31.5$ cm, $h_l = 5.5$ cm and $h_c = 14.5$ cm. w is chosen as mentioned above. Here, δ' and δ will be in centimeters. Observe that, δ' vs d is almost linear and δ vs d is linear.

So far the analysis made for finding depth of both dry and water-filled potholes is based on measurements δ and δ' in physical units. However, in reality we measure δ and δ' in

Fig. 7: Zero crossing region of quartic function (34).

Fig. 9: Change of resolution of camera with distance.

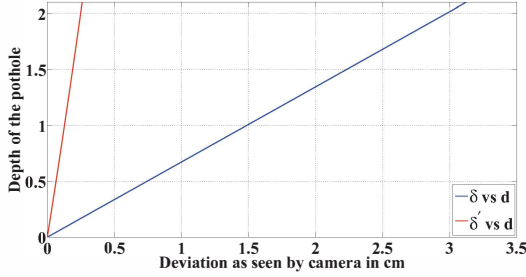Fig. 8: d vs δ (blue) and d vs δ' (red).

Fig. 10: d vs δ_p (blue) and d vs δ'_p (red).

pixels. Therefore, relation between pixels and physical units need to be established. Our analysis assumes that image point where the laser ray hits the road surface (without any pothole) coincides with the principal point of the camera. Under this assumption we can relate δ and δ' in physical units to pixel units as follows:

$$\delta_p = R_s\delta, \tag{37}$$

where δ_p is deviation in pixels, δ is deviation in cm and R_s is resolution of camera for distance r_d of imaging plane (plane parallel to image plane at which point of interest lies) from camera and is given by

$$R_s = \frac{f}{r_d}, \tag{38}$$

where f is the focal length of the camera. Without a pre-calibrated camera, we next estimate the focal length f from empirical observations of resolution at various distances (r_d's) from the camera plane. To such data, we then fit the least-squared estimate, $\arg\min_f \sum_{i=1}^{N_d}(R_s^i - \frac{f}{r_d^i})^2$, where N_d is number of observations. Fig. 9 gives both observed and least square fit plot for R_s vs r_d.

Now we can plot for δ'_p vs d and δ_p vs d considering the respective r_d of dry and water filled potholes, expression for which are given below. For dry pothole, from $\triangle$AQP

$$r_d = \sqrt{(h_c + d)^2 + (R + d\tan\theta_l)^2} \tag{39}$$

and for water-filled pothole, from $\triangle$AOL

$$r_d = \sqrt{(h_c + d_c)^2 + ((h_c + d_c)\tan\theta'_c)^2}. \tag{40}$$

Fig 10 shows the plots for both δ'_p vs d and δ_p vs d considering the same parameter as that of Fig. 8. Observe that δ'_p vs d

in this case is almost linear where as δ_p vs d is nonlinear. Finally, Fig 10 is used to find depths of both dry and water-filled potholes for the measurements δ_p and δ'_p.

IV. EXPERIMENTAL VERIFICATION

In this section, we corroborate our mathematical analysis with experimental data. We first discuss the experimental setup, followed by detection of pothole and then finally estimation of the actual depth of the pothole.

A. Description of the prototype

The complete experimental setup includes a vehicle (toy car), a laser source (line source) operating in visible spectrum (red light) and a camera (Microsoft HD LifeCam) arranged as shown in Fig. 11. Camera is fixed on top of the laser source and is aligned vertically with the laser. Road surface is simulated by using a metal sheet on which channels of known fixed depths are made which are considered as potholes. We considered three potholes of depths 10 mm, 15 mm and 20 mm for experimental verification. For this setup $R = 31.5$ cm, $h_l = 5.5$ cm and $h_c = 14.5$ cm.

B. Detection of the pothole

The laser source projects a laser onto the metal sheet with pothole and then camera captures the image of the laser. Laser line captured by camera is separated from the background using thresholding operation [6]. The binary output is compared with the reference template to detect the deformation. The template consists of image of laser line on road without pothole. The template image and its binary version can be seen in Fig. 12. A mismatch immediately indicates the unevenness of the road, possibly a pothole.
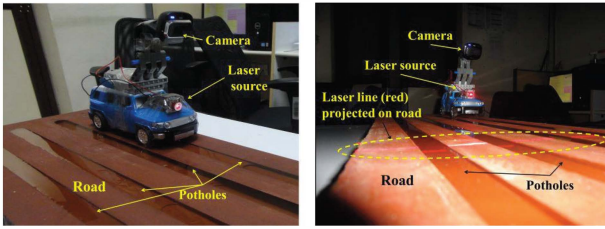
Fig. 11: Front view and side view of experimental setup

Pothole depth (mm)	Optical deviation (pixels)	
	δ_p	δ'_p
10	89.5	10
15	126.5	12
20	156.5	15

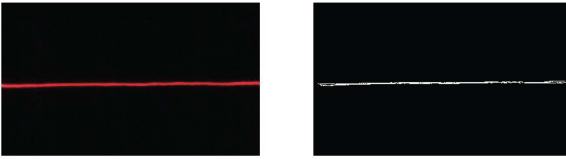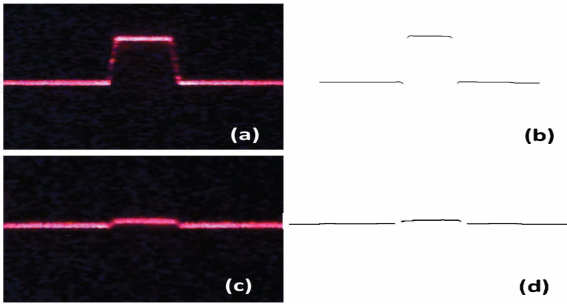TABLE I: Measured δ_p and δ'_p from the images captured.

Fig. 12: Template image

Fig. 13: (a), (c): Captured dry and water-filled pothole of $d = 20mm$; (b), (d) corresponding binary image used to calculate optical deviation.

C. Estimation of depth of pothole

Finally, δ_p for dry pothole and δ'_p for water-filled pothole are measured in pixels for all potholes (refer to Table I). Subsequently, these values are compared with reference chart (shown in Fig. 10) to estimate the actual depth d of the pothole. Table II presents actual and estimated values of depths for representative potholes in dry and water-filled case.

Observe that estimated depth matches closely with actual depth for dry potholes with around 1% error. However, for water-filled potholes, deviation is larger from actual depths with varying error (5% to 17 %) (refer to Table II). Such larger deviation is likely in large part the result of curvature of the water surface due surface tension. However, in actual application on road, the pothole depth and width will potentially be much larger, and the above effect should be minimal, leading to better accuracy.

Actual depth (mm)	Estimated depth (mm)			
	Dry pothole	% error	Water-filled pothole	% error
10	10.1	1	11.7	17
15	15.2	1.33	14.2	5.33
20	20.2	1	18.1	9.5

TABLE II: Comparison between actual and estimated depths.

V. DISCUSSION

This paper presents a physics-based geometric method to determine pothole depth, both in dry and water-filled conditions. While the analysis for dry potholes is straightforward, that for water-filled ones is considerably involved. Importantly, based on our analysis, an automated and inexpensive image-based system can be implemented practically. Towards this, we demonstrate a proof of principle via a scaled-down experiment. However, crucial challenges still remain towards productization. For instance, the laser and camera angles may vary statistically within a limit, and one should translate our analysis to a probabilistic framework. Several other engineering parameters, such as laser frequency and wattage, camera resolution and frame rate, need to be optimized in the real-life deployment in terms of performance-cost tradeoff. Of course, determining whether the detected pothole is dry or water filled can be made reliable by appropriate use of machine learning methods. The maximum speed that a vehicle can maintain for a given system to work would also be a crucial factor. Finally, pothole information can be shared via communication links, thereby improving collective driving experience.

REFERENCES

[1] A. Boukerche, H. A. B. F. Oliveira, E. F. Nakamura, A. A. F. Loureiro, "Vehicular Ad Hoc Networks: A New Challenge for Localization-Based Systems," *Computer Communications*, 2008.

[2] J. Eriksson, L. Girod, B. Hull, R. Newton, S. Madden, H. Balakrishnan, "The Pothole Patrol: Using a Mobile Sensor Network for Road Surface Monitoring," *Proceedings of the 6th International Conference on Mobile Systems, Applications, and Services*, pp. 29–39, 2008.

[3] G. Strazdins, A. Mednis, G. Kanonirs, R. Zviedris, L. Selavo, "Towards Vehicular Sensor Networks with Android Smartphones for Road Surface Monitoring," *Institute of Electronics and Computer Science,* University of Latvia.

[4] S. Rode, S. Vijay, P. Goyal, P. Kulkarni, K. Arya, "Pothole Detection and Warning System: Infrastructure Support and System Design," *International Conference on Electronic Computer Technology*, pp.286–290, Feb. 2009.

[5] S. Vijay, "Low Cost – FPGA based system for pothole detection on Indian Roads", *M-Tech Thesis, Indian Institute of Technology Bombay*, Jul. 2006.

[6] X. Yu, E. Salari, "Pavement Pothole Detection and Severity Measurement Using Laser Imaging," *IEEE International Conference on Electro/Information Technology (EIT)*, pp. 1–5, May 2011.

[7] C. Mertz, "Continuous Road Damage Detection Using Regular Service Vehicles", *Proceedings of the ITS World Congress, Carnegie Mellon University*, Oct. 2011.

[8] N. Angelini, M. Gdula, C. Shelvin, J. Brache, "Mapping city potholes", *Project Report, Department of Computer Engineering, Worcester Polytechnic Institute*, Apr. 2006.

[9] http://www.lsbu.ac.uk/water/vibrat.html

[10] http://planetmath.org/QuarticFormula